

# Single-molecule nanocatalysis reveals heterogeneous reaction pathways and catalytic dynamics

Weilin Xu, Jason S. Kong, Yun-Ting E. Yeh, Peng Chen<sup>†</sup>

Department of Chemistry and Chemical Biology, Cornell University, Ithaca, NY 14853, USA

<sup>†</sup> To whom correspondence should be addressed. E-mail: pc252@cornell.edu

## 1. Single-nanoparticle catalysis experiments.

Single-molecule fluorescence measurements were performed on a homebuilt prism-type total internal reflection (TIR) fluorescence microscope based on an Olympus IX71 inverted microscope. A continuous wave circularly polarized 532 nm laser beam (CrystaLaser, GCL-025-L-0.5%) of 1.5-3 mW was focused onto an area of  $\sim 80 \times 40 \mu\text{m}^2$  on the sample to directly excite the fluorescence of resorufin. The fluorescence of resorufin was collected by a 60X NA1.2 water-immersion objective (UPLSAPO60XW, Olympus), filtered by two filters (HQ550LP, HQ580m60), and projected onto a camera (Andor iXon EMCCD, DV887DCS-BV), which is controlled by an Andor IQ software. An additional 1.6X magnification on the microscope is also used sometimes. All optical filters are from Chroma Technology Corp. The movies are analyzed using a home-written IDL program, which extracts the fluorescence intensity trajectories from localized fluorescence spots individually across the entire movie. The intensity of each bright spot in an image is obtained by integrating the signal counts over an area of  $\sim 1 \times 1 \mu\text{m}^2$ .

A flow cell,  $100 \mu\text{m}$  (height)  $\times$   $2 \text{ cm}$  (width)  $\times$   $5 \text{ mm}$  (length), formed by double-sided tapes sandwiched between a quartz slide (Technical Glass or Finkenbeiner) and a borosilicate coverslip (Gold Seal<sup>®</sup>), was used to hold aqueous sample solutions for single-nanoparticle single-molecule fluorescence measurements. Before being assembled into a flow cell, the quartz slide was amine-functionalized by an aminoalkylsiloxane reagent (Vectabond, Vector Laboratory), whose amine functional group is protonated, thus positively charged in water.  $100 \mu\text{L}$  of  $1 \text{ nM}$  colloidal Au-nanoparticle solution was then added onto the slide, and incubated for 30 minutes. The slide was then rinsed for 3 minutes with MilliQ water to wash away the unbound Au-nanoparticles. These colloidal Au-nanoparticles were prepared from citrate reduction of  $\text{HAuCl}_4$ ; they are negatively charged and known to be immobilized on positively charged surfaces<sup>S1,2,3</sup>. On the quartz slide two holes were drilled to connect to polyethylene tubing and a syringe pump for continuous solution flow at  $5 \mu\text{L}/\text{minute}$ .

## 2. Au-nanoparticles and characterization.

We experimented with both commercial (Ted Pella) and homemade spherical colloidal Au-nanoparticles with 2, 6, 10, 13 and 14 nm diameters, all prepared from citrate reduction of  $\text{HAuCl}_4$  in aqueous solutions<sup>S1</sup>. These Au-nanoparticles, except the 2-nm ones, show the characteristic wine-red color and are stable over months stored at  $4^\circ\text{C}$ . Figure S1A shows the TEM image (taken with FEI

Tecnai 12) of the 6-nm colloidal Au-nanoparticles (Ted Pella) that we focus on in the current study. The determined average diameter and size dispersion are  $6.0 \pm 1.6$  nm (Figure S1B).

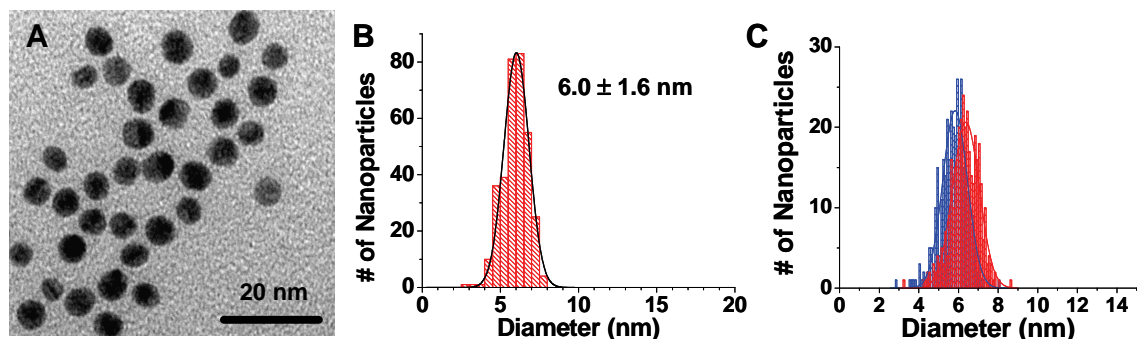


**Figure S1.** TEM image (A) and size distribution (B) of the 6-nm spherical colloidal Au-nanoparticles. (C) Distributions of maximum diameter (red,  $6.4 \pm 1.3$  nm) and minimum diameter (blue,  $5.8 \pm 1.2$  nm) of the 6-nm Au-nanoparticles.

### 3. Ensemble measurements of Au-nanoparticle catalyzed reduction of resazurin to resorufin.

We tested the ability of the Au-nanoparticles in catalyzing the reduction of resazurin to resorufin in ensemble measurements. The catalytic reactions were carried out in water at room temperature, initiated by injection of an aliquot of Au-nanoparticle solution into a premixed solution of resazurin (Molecular Probes, Invitrogen) and a large excess of  $\text{NH}_2\text{OH}$  (J. T. Baker), and monitored by UV-Vis absorption. The 6, 10, 13, and 14 nm Au-nanoparticles are all active, while the 2-nm Au-nanoparticles are inactive in catalyzing the reduction of resazurin by  $\text{NH}_2\text{OH}$ . We focus on the 6-nm Au-nanoparticles in this study.

Upon injection of Au-nanoparticles, the solution color turns from blue (resazurin) to red (resorufin) gradually. The absorption spectrum of the reaction solution shows over time a decrease of the resazurin absorption at 598 nm and an increase of the resorufin absorption at 568 nm (Figure S2A). The plasmon band of the Au-nanoparticle is not observable at low comparative concentration. An isosbestic point is clear in the absorption spectra, indicating the quantitative conversion of resazurin to resorufin catalyzed by Au-nanoparticles. This quantitative conversion is clearer in the time profiles of the absorbance at 568 and 598 nm (Figure S2B), showing the direct correlation between resazurin consumption and resorufin production. The product of  $\text{NH}_2\text{OH}$  oxidation in this catalytic reaction is probably nitrite ( $\text{NO}_2^-$ ) or related products<sup>S4</sup>, which is not the focus of our study.

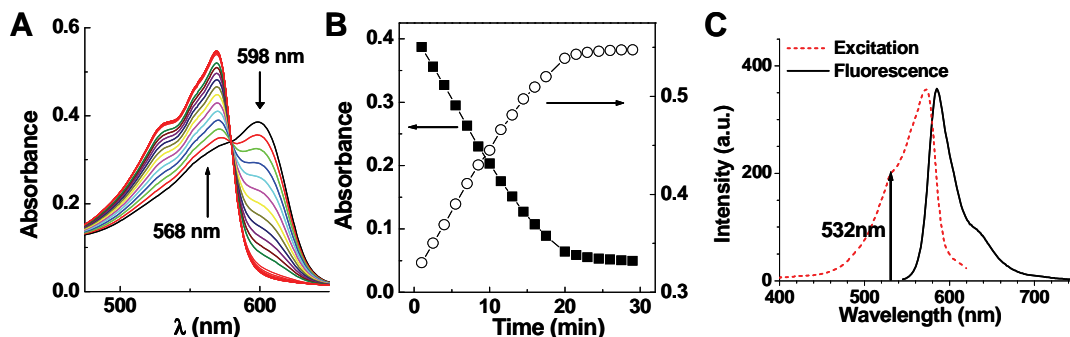


**Figure S2.** (A) In situ absorption measurements of resazurin reduction by  $\text{NH}_2\text{OH}$  catalyzed by Au nanoparticles in aqueous solution.  $[\text{resazurin}]_0 = 8 \mu\text{M}$ ;  $[\text{NH}_2\text{OH}]_0 = 160 \mu\text{M}$ ;  $[\text{Au nanoparticle}] = 0.02$

$\mu\text{M}$ . (B) Time profiles of absorbance at 598 and 568 nm from (A). (C) Excitation and fluorescence (excited at 532 nm) spectra of resorufin.

As a control, no indication of resazurin reduction by  $\text{NH}_2\text{OH}$  was observed without Au-nanoparticles over a few hours from absorption measurements at similar conditions. Consistently, without  $\text{NH}_2\text{OH}$ , Au-nanoparticles cannot effect resazurin reduction.

Figure S2C shows the excitation and fluorescence spectra of resorufin in water. Resorufin is a highly fluorescent molecule with large extinction coefficients ( $\epsilon_{570\text{ nm}} \sim 57000\text{ M}^{-1}\text{cm}^{-1}$ ) and a high fluorescence quantum yield (up to 0.97 at neutral to basic conditions)<sup>S5</sup>. The fluorescence of resorufin is readily excited at 532 nm. In contrast, the substrate resazurin has smaller extinction coefficients ( $\epsilon_{570\text{ nm}} \sim 32000\text{ M}^{-1}\text{cm}^{-1}$ ) and a much lower fluorescence quantum yield ( $<0.1$ )<sup>S6</sup>. The highly fluorescent nature of the product resorufin and the nonfluorescent nature of the substrate resazurin form the basis for our single-molecule fluorescence detection of single turnovers catalyzed by Au-nanoparticles (Figure 1a).

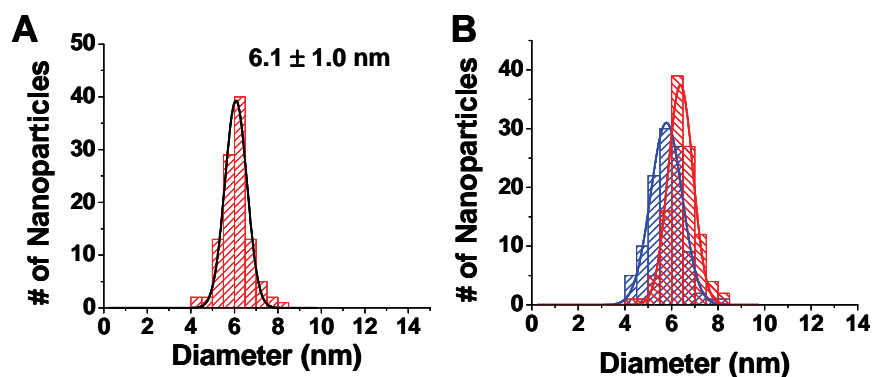
#### 4. TEM characterization of 6-nm Au-nanoparticles before and after catalysis.

The 6-nm Au-nanoparticles are not perfectly spherical (Figure S1A). To examine the effects of catalysis on the size and shape of 6-nm Au nanoparticles, we attempted to measure the maximum diameter and minimum diameter of each Au-nanoparticle in the TEM images, and built distributions for both.

Figure S1C shows the distributions of maximum and minimum diameters of the 6-nm Au-nanoparticles before undergoing catalysis. The mean maximum and minimum diameters are  $6.4 \pm 1.3$  and  $5.8 \pm 1.2$  nm. The aspect ratio is  $\sim 0.91$  (minimum/maximum).

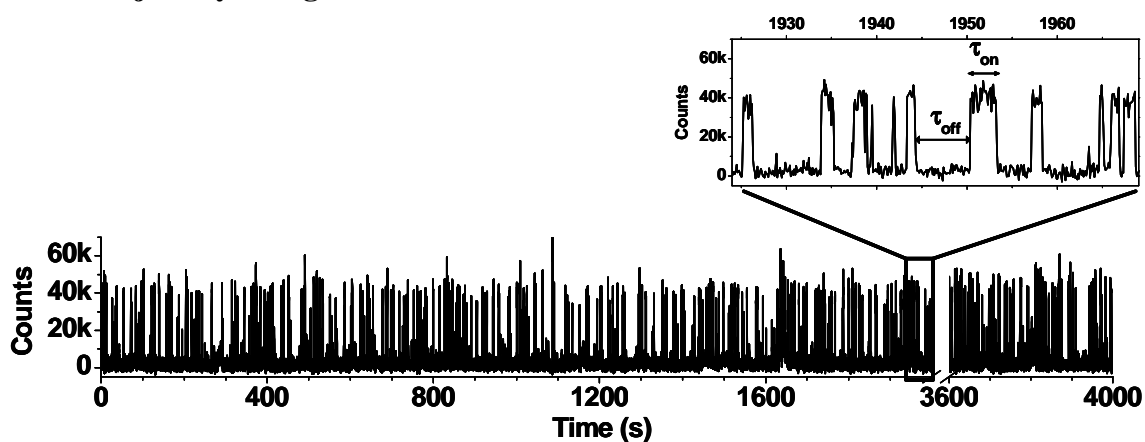
We then carried catalytic reactions as described earlier and analyzed the Au-nanoparticles afterwards with TEM measurements. We controlled the resazurin/Au-nanoparticle ratio in the catalytic reactions to ensure that each nanoparticle undergoes similar number of turnovers as those in our single-nanoparticle experiments.

Figure S3A shows the mean size distribution of the Au-nanoparticles after catalysis. The measured mean diameter is  $6.1 \pm 1.0$  nm, same as that before catalysis within experimental error. Figure S3B shows the distributions of the maximum and minimum diameters with mean at  $6.4 \pm 1.1$  nm, and  $5.8 \pm 1.4$  nm, respectively. The aspect ratio is  $\sim 0.91$ , indistinguishable from that before catalysis.



**Figure S3.** (A) Size distribution of the 6-nm Au nanoparticles after catalysis. (B) Distributions of maximum (red,  $6.4 \pm 1.1$  nm) and minimum (blue,  $5.8 \pm 1.4$  nm) diameters of Au-nanoparticles after catalysis.

### 5. Full trajectory of Figure 1c.



**Figure S4.** Fluorescence trajectory from which the segment in Figure 1C in the main text was taken.

## 6. Control experiment with pure resorufin.

The resazurin sample we used contains 1% resorufin contamination. To rule out that binding or unbinding of free resorufin in the solution to a Au-nanoparticle is the cause of the burst behavior of fluorescence trajectories, we performed control experiments with only resorufin in solution at 1% of the concentrations of resazurin used for catalysis. No digital burst fluorescence trajectories were observed. This indicates that at these resorufin concentrations (up to  $\sim 10^{-8}$  M), binding of resorufin to Au-nanoparticle surface is insignificant in our single-nanoparticle catalysis experiments. Note that in the single-nanoparticle catalysis experiment, the resorufin is generated *in situ* from *pre-adsorbed* resazurin, which does not involve a resorufin-binding process.

Simple diffusion of free resorufin in the solution should not be the cause of the digital trajectories, as the diffusion time of a small molecule within the TIR excitation region ( $\sim 200$  nm thick above the surface) is on the  $\mu$ s timescale, much shorter than the 30-100 ms imaging frame time in our experiments. For the same reason, free resorufin in the solution is not detectable in single-molecule fluorescence imaging because of its fast diffusion.

Fluorescence blinking of a resorufin molecule permanently bound to a Au-nanoparticle cannot be the cause of the fluorescence bursts in our single-nanoparticle experiment for several reasons: (1) a single resorufin molecule will be photobleached in tens of seconds (photobleaching lifetime of resorufin is  $\sim 25$  s (Figure S6), while our single-nanoparticle catalysis movies are about one hour long; (2) blinking would be laser intensity dependent, but our single-nanoparticle catalysis turnovers are not (Figure S5); and (3) fluorescence bursts were not observed in our control experiments with pure resorufin solution over Au-nanoparticles.

## 7. The laser intensity dependence of $\langle \tau_{\text{off}} \rangle^{-1}$ and $\langle \tau_{\text{on}} \rangle^{-1}$ .

To show that the catalysis of Au-nanoparticles is not photoinduced, we measured the laser intensity dependence of  $\langle \tau_{\text{off}} \rangle^{-1}$  and  $\langle \tau_{\text{on}} \rangle^{-1}$ . As shown in Figure S5,  $\langle \tau_{\text{off}} \rangle^{-1}$  and  $\langle \tau_{\text{on}} \rangle^{-1}$  are independent of the laser intensity in the range used in our single-nanoparticle catalysis experiments.

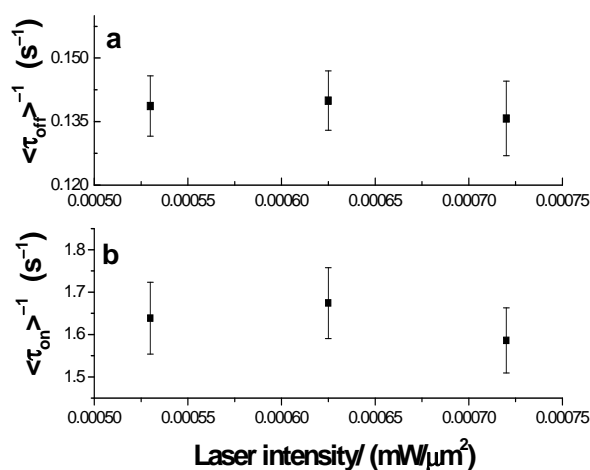


**Figure S5.** Laser intensity dependence of  $\langle \tau_{\text{off}} \rangle^{-1}$  and  $\langle \tau_{\text{on}} \rangle^{-1}$  at  $[S] = 10^{-7}$  M and  $[\text{NH}_2\text{OH}] = 1.0$  mM.

## 8. Control experiment on resorufin photobleaching.

We measured the photobleaching lifetime of resorufin. We immobilized resorufin molecules in a polymethyl-methacrylate (PMMA) (Aldrich) film by spin-coating 20  $\mu\text{L}$  of 50 pM solution of resorufin in PMMA in toluene onto a slide according to literature procedures<sup>S7</sup>. A  $\sim 10\ \mu\text{m}$  water layer was then added on top of the PMMA film to provide an approximate aqueous environment. An uncoated coverslip was then used to sandwich sample for measurements on our TIR fluorescence microscope.

We excited resorufin with laser intensity of  $\sim 6.25 \times 10^{-4}\ \text{mW}/\mu\text{m}^2$ , the same laser intensity used for single-nanoparticle catalysis experiments. Figure S6A shows exemplary fluorescence trajectories of single resorufin molecules with single-step photobleaching. The average of the photobleaching of about 100 resorufin molecules is  $\sim 28\ \text{s}$ . Figure S6B is the distribution of the photobleaching lifetimes of resorufin molecules. It can be fitted by a single-exponential decay function with a time constant of  $\sim 25\ \text{s}$ . Both the average photobleaching lifetime and the time constant from fitting the distribution are significantly larger than the average  $\tau_{\text{on}}$  in our single-turnover trajectories. Therefore, photobleaching does not contribute to the distribution of  $\tau_{\text{on}}$  in our catalysis experiments.

Furthermore, the independence of  $\langle \tau_{\text{on}} \rangle^{-1}$  on the laser intensity also indicates that resorufin photobleaching is insignificant in our single-nanoparticle catalysis experiments (Figure S5).

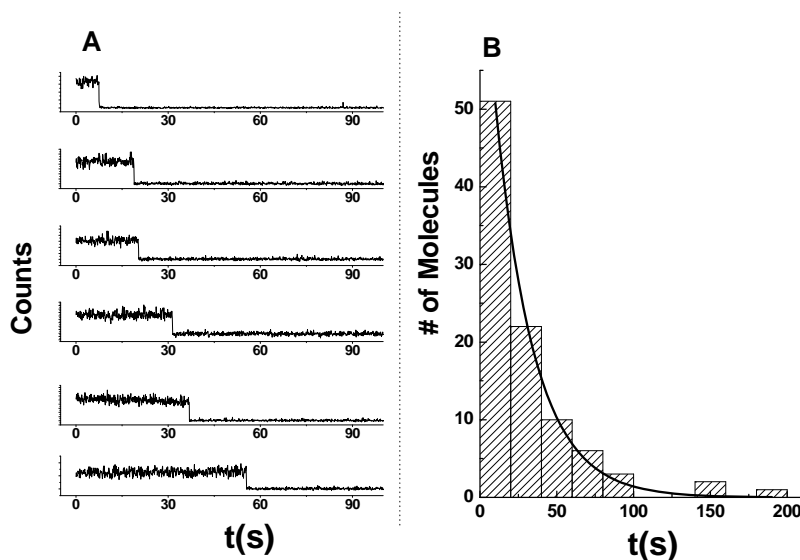


**Figure S6.** (A) Typical fluorescence intensity trajectories for single resorufin photobleaching. (B) Distribution of lifetimes before photobleaching of resorufin molecules. Solid line is a single-exponential decay fit with a time constant of  $\sim 25\ \text{s}$ .

## 9. $\text{NH}_2\text{OH}$ concentration dependence of catalysis kinetics.

We performed control experiments with variable  $\text{NH}_2\text{OH}$  concentrations (0.8 – 1.2 mM) at 0.1  $\mu\text{M}$  resazurin and laser intensity of  $6.23 \times 10^{-4}\ \text{mW}/\mu\text{m}^2$ . Figure S7 shows that at this large excess of  $\text{NH}_2\text{OH}$ , the catalytic kinetics is independent of the  $\text{NH}_2\text{OH}$  concentration.

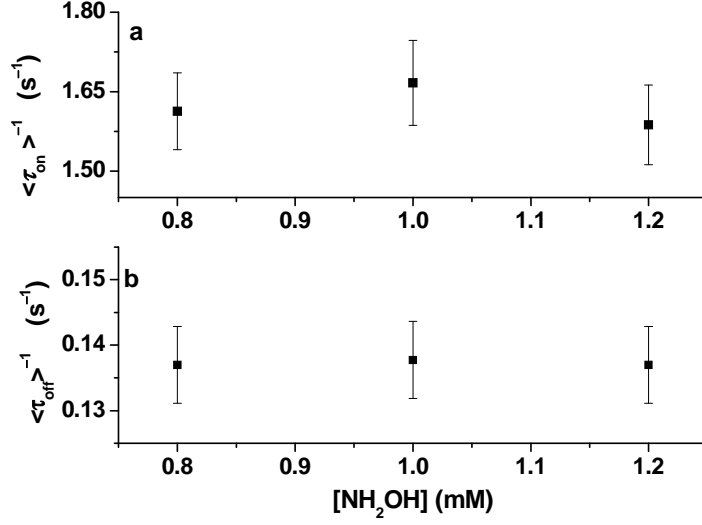


**Figure S7.** The  $\text{NH}_2\text{OH}$  concentration dependence of  $\langle \tau_{\text{on}} \rangle^{-1}$  and  $\langle \tau_{\text{off}} \rangle^{-1}$ .

### 10. Averaging of three types of Au-nanoparticles in Figure 3a and b.

Figure S8 shows the averaged result of the three types of Au-nanoparticles. The heterogeneity in catalysis and differentiation of the subpopulations are masked, and the  $\langle \tau_{\text{on}} \rangle^{-1}$  behavior is dominated by type-I Au-nanoparticles.

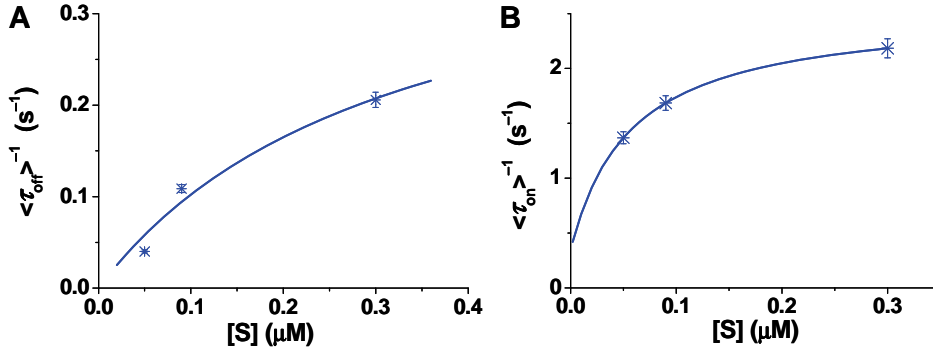


**Figure S8.**  $[\text{S}]$  dependence of  $\langle \tau_{\text{off}} \rangle^{-1}$  (A) and  $\langle \tau_{\text{on}} \rangle^{-1}$  (B) averaged over all three types of Au-nanoparticles. Total number nanoparticles: 61. Solid lines are simulations of Equations (1) and (2) with  $\gamma_{\text{eff}} = 0.4 \text{ s}^{-1}$ ,  $K_1 = 3.1 \text{ } \mu\text{M}^{-1}$ ,  $k_2 = 2.5 \text{ s}^{-1}$ ,  $K_2 = 11.7 \text{ } \mu\text{M}^{-1}$ , and  $k_3 = 0.34 \text{ s}^{-1}$ .

### 11. The laser excitation intensity control of activity fluctuations during $\tau_{\text{off}}$ and $\tau_{\text{on}}$ reactions.

To show that the fluctuations of Au-nanoparticle activity are not photoinduced, we studied the laser intensity dependence of the correlation time  $m_{\text{off}}\tau_{\text{on+off}}$  and  $m_{\text{on}}\tau_{\text{on+off}}$  from the autocorrelation functions of  $\tau_{\text{off}}$  and  $\tau_{\text{on}}$ . As shown in Figure S9,  $\langle m_{\text{off}}\tau_{\text{on+off}} \rangle$  and  $\langle m_{\text{on}}\tau_{\text{on+off}} \rangle$  are independent of the laser intensity in the range used in our single-nanoparticle catalysis experiments.

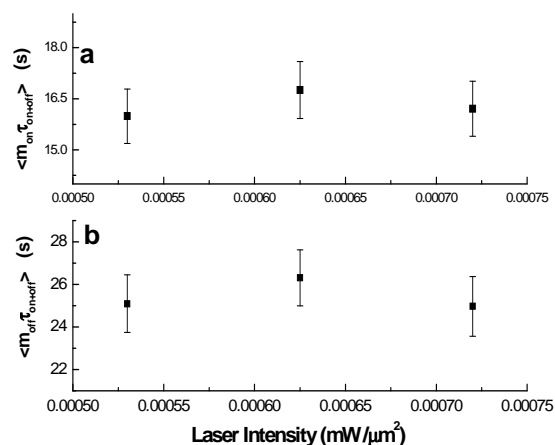


**Figure S9.** Laser intensity dependence of  $\langle m_{\text{off}} \tau_{\text{on+off}} \rangle$  and  $\langle m_{\text{on}} \tau_{\text{on+off}} \rangle$  at  $[S]=10^{-7}$  M and  $[\text{NH}_2\text{OH}]=1.0\text{mM}$ .

## 12. Dependence of the activity fluctuation rates on the rate of turnovers for three types of the Au-nanoparticles.

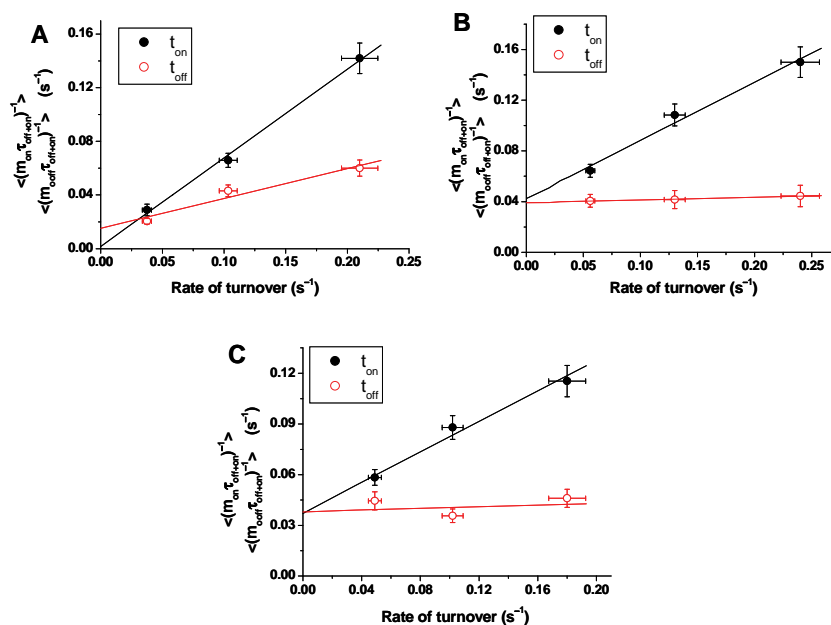


**Figure S10.** Dependence of the activity fluctuation rates on the rate of turnovers for type-I (A), type-II (B) and type-III (C) Au-nanoparticles. The solid lines are linear fits. The intercepts on the y-axis are: (A)  $0.015 \pm 0.007 \text{ s}^{-1}$  for  $\tau_{\text{off}}$  reactions,  $0.002 \pm 0.006 \text{ s}^{-1}$  for  $\tau_{\text{on}}$  reactions. (B)  $0.039 \pm 0.001 \text{ s}^{-1}$  for  $\tau_{\text{off}}$  reactions,  $0.04 \pm 0.01 \text{ s}^{-1}$  for  $\tau_{\text{on}}$  reactions. (C)  $0.038 \pm 0.007 \text{ s}^{-1}$  for  $\tau_{\text{off}}$  reactions,  $0.038 \pm 0.007 \text{ s}^{-1}$  for  $\tau_{\text{on}}$  reactions.

## 13. Substrate migration as a potential cause of activity fluctuation

There are many catalytic sites on one Au-nanoparticle. If these sites have different activities, substrate migration among different sites on the same nanoparticle could lead to temporal variations of reaction rates. The correlation time of the activity fluctuation would then be the timescale for surface substrate migration. This effect should diminish, however, at saturating substrate concentrations where

every surface site is occupied. Experimentally, the activity fluctuation rates increase with increasing rates of turnovers, i.e., increasing substrate concentrations (Figure 4d). This dependence thus ruled out substrate migration as the cause of the activity fluctuation of individual Au-nanoparticles.

#### 14. The cross correlation of $\tau_{\text{off}}$ and $\tau_{\text{on}}$ .

Figure S11 shows the cross correlation function of  $\tau_{\text{off}}$  and  $\tau_{\text{on}}$  derived from the same single-turnover trajectory as that of  $r(t)$  in Figure 4a. No cross correlation was discernible between  $\tau_{\text{off}}$  and  $\tau_{\text{on}}$ .

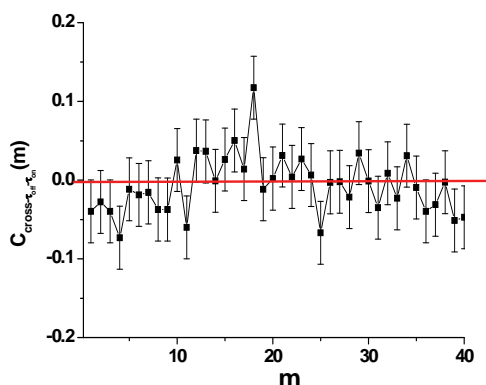


**Figure S11.** Cross correlation function of  $\tau_{\text{off}}$  and  $\tau_{\text{on}}$  derived from the same trajectory as that of  $r(t)$  in Figure 4a.

#### 15. Collisional fluorescence quenching of resorufin by Au-nanoparticles in solution.

Under certain conditions, metal-nanoparticles are known to quench the fluorescence of small molecules through either collisional quenching or static quenching, the latter of which would affect our single-molecule detection of the catalytic product resorufin that is adsorbed on the Au-nanoparticle. To probe the possible quenching effects of Au-nanoparticles on resorufin fluorescence, we measured the resorufin fluorescence in solution in the presence of 1 mM  $\text{NH}_2\text{OH}$ , which is used in our single-nanoparticle experiments, and of increasing concentrations of Au-nanoparticles.

Figure S12 shows the Stern-Volmer plots of resorufin quenching by Au-nanoparticles in solution at two different temperatures<sup>S8,9</sup>. The slopes in both lines represent the quenching efficiencies, and their positive values indicate the Au-nanoparticle can indeed quench the fluorescence of resorufin in solution. However, with increasing temperature, the slope in the Stern-Volmer plots increases, indicating that the fluorescence quenching here is due to collisional quenching—the fluorescence energy is transferred by collision between the free resorufin and the Au-nanoparticles in solution<sup>S8,9</sup>. In our single-nanoparticle experiments, the resorufin is catalytically generated in situ from pre-adsorbed resazurin and detected while still adsorbed on a Au-nanoparticle surface; thus, there is no collision between the resorufin molecule and the Au-nanoparticle. The lack of collisional quenching in our single-nanoparticle catalysis experiments is consistent with that we can detect the resorufin fluorescence at the single-molecule level adsorbed on Au-nanoparticles.

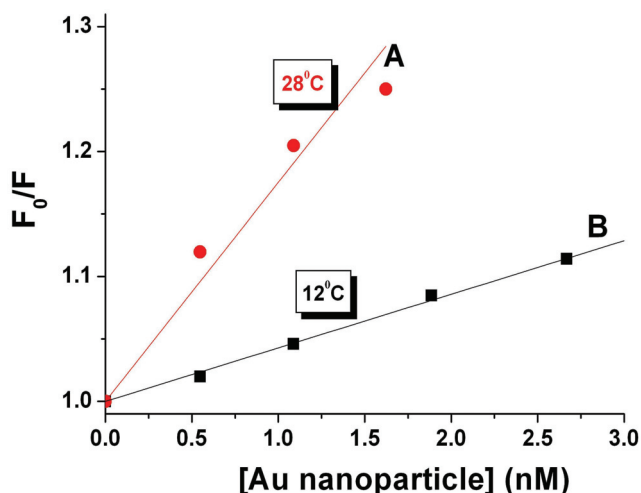


**Figure S12.** The quenching Stern-Volmer plots for resorufin at different 6-nm Au-nanoparticle concentrations at 28°C (A) and 12°C (B).  $F_0$  is the fluorescence intensity of resorufin in the absence of Au-nanoparticles.  $F$  is the intensity in the presence of various concentrations of Au-nanoparticles. Resorufin concentration is at 100 nM.

## 16. Deactivation of Au-nanoparticle after long period of reaction time

We found that the activity of Au-nanoparticles decreases gradually over extended reaction time, which becomes significant after about  $\sim 4$  hours (Figure S13), possibly due to catalysts deactivation/poisoning. To ensure that catalyst deactivation does not affect our experimental data, all single-nanoparticle experiments were carried out within 3 hours after the initiation of catalysis. This constraint limited the number of different concentrations used in measuring the catalysis of the same set of Au-nanoparticles, where each concentration takes 1 hour to acquire long single-turnover trajectories that have statistically significant number of turnover events.

We also determined the substrate concentration dependence of  $\langle \tau_{\text{off}} \rangle^{-1}$  and  $\langle \tau_{\text{on}} \rangle^{-1}$ , by analyzing only the first 15 minutes of every turnover trajectory (Figure S13B, C). The results are similar to those in Figure 2a, b in the main text.

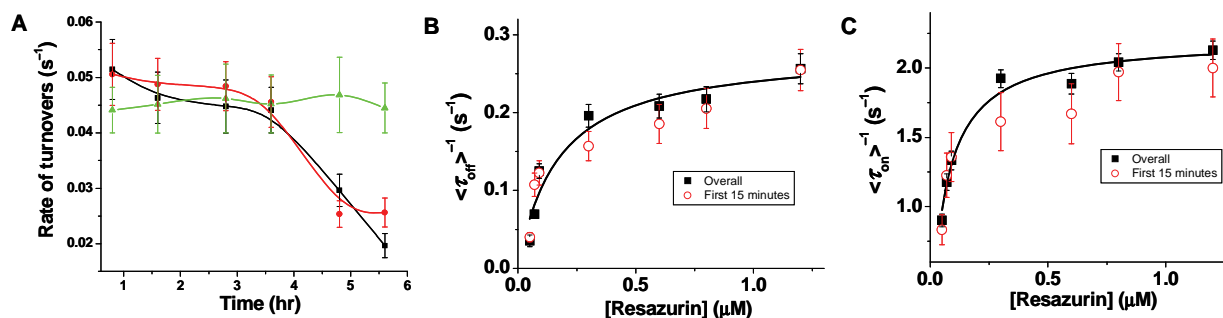


**Figure S13.** (A) Time-dependent rate of turnovers for three Au-nanoparticles at 0.05  $\mu\text{M}$  resazurin and 1 mM  $\text{NH}_2\text{OH}$ . Every data point was an average of the turnover events in a segment of trajectory of  $\sim 33$  minutes. (B) Nanoparticle-averaged  $[S]$  dependence of  $\langle \tau_{\text{off}} \rangle^{-1}$ . (C) Nanoparticle-averaged  $[S]$  dependence of  $\langle \tau_{\text{on}} \rangle^{-1}$ . Every data point in (B, C) is calculated by analyzing the first 15 minutes of every turnover trajectory. Data from Figure 2a, b are also plotted in (B, C).

## 17. Possible contribution of reaction heat to activity fluctuations

During catalysis, the heat released by the reaction at one site could affect the reactivity of neighboring sites, which could contribute to the temporal activity fluctuations of a single Au-nanoparticle. However, this possibility is unlikely the main reason for the activity fluctuations. From Figure 4d and Figure S10, the positive intercepts of fluctuation rates at zero rate of turnovers indicate that when no reaction happens (thus no heat releases), the underlying dynamics still occur. This is attributable to spontaneous (as compared to catalysis-induced) surface restructuring dynamics.

## 18. Derivation of single-molecule kinetics equations.

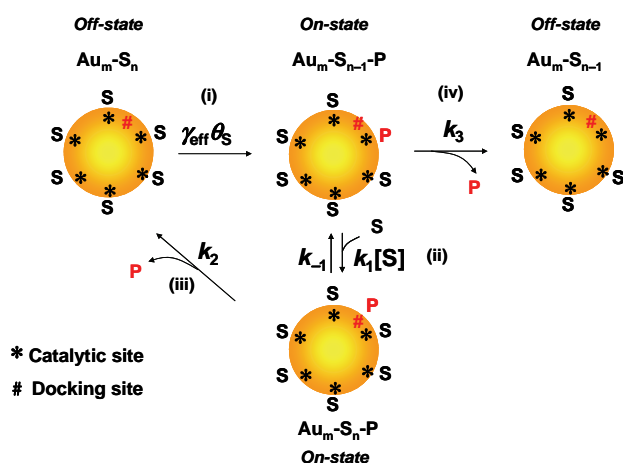


**Figure S14.** Kinetic mechanism of Au-nanoparticle catalyzed resazurin reduction to resorufin, as described in Figure 2c.

### Part A: Derivation of the distribution of the off-time $f_{off}(\tau)$ , and of $\langle \tau_{off} \rangle^{-1}$ .

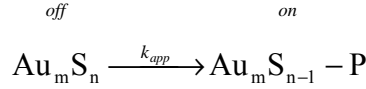
The single-turnover trajectories such as that in Figure 1C cleanly separate the catalysis into two parts: the  $\tau_{off}$  process and the  $\tau_{on}$  process. The stochastic quantity  $\tau_{off}$  is the waiting time before each product formation. At the start of each  $\tau_{off}$ , no product has yet formed on the nanoparticle surface; as soon as a product is formed,  $\tau_{off}$  ends and  $\tau_{on}$  starts. To analyze the statistical properties of  $\tau_{off}$ , we considered a Langmuir-Hinshelwood mechanism well-known in heterogeneous catalysis<sup>S10</sup>. This mechanism assumes:

(i) Independent and uniform sites on the surface of each nanoparticle. In reality, there are different surface sites on each nanoparticle; however, as our experiments only have single-particle resolution, not single-site resolution, the single-particle kinetic parameters are averaged properties of the many sites on *each particle*. The assumption of “uniform sites” is thus a valid approximation within our experimental limitation.

(ii) Quasi-equilibrium in adsorption of substrate on the sites (i.e., substrate molecules bind to the Au-nanoparticle reversibly and a fast adsorption equilibrium is established at all times). The surface coverage of substrate molecules here is determined by the adsorption equilibrium governed by the Langmuir isotherm<sup>S10</sup>.

(iii) Rapid dissociation of product from nanoparticle surface, as compared to the rate of catalytic conversion. This assumption is consistent with our experimental results that the average off-time  $\langle \tau_{off} \rangle$ , which contains the catalytic conversion reaction, is much longer than the average on-time  $\langle \tau_{on} \rangle$ , which contains the product dissociation reaction (Figure 2a and 2b).

Based on this mechanism, the reaction taking places during  $\tau_{\text{off}}$  is the following (Figure S14):



where  $n$  is the number of resazurin substrate molecules adsorbed on the nanoparticle surface,  $\text{Au}_m$  stands for the Au-nanoparticle, S for the substrate resazurin, P for the product resorufin, and  $k_{\text{app}}$  is the apparent rate constant for forming one product on the surface of one nanoparticle. Here the formation of a P and thus of the state  $\text{Au}_m\text{S}_{n-1}-\text{P}$  marks the completion of a  $\tau_{\text{off}}$ . From Langmuir-Hinshelwood kinetics for heterogeneous catalysis<sup>S10</sup>,  $k_{\text{app}}$  takes the form:

$$k_{\text{app}} = k_i k' n$$

Here  $k_i$  is the rate constant representing the intrinsic reactivity per catalytic site for the catalytic conversion reaction.  $k'$  is a quantity accounting for the contribution of  $\text{NH}_2\text{OH}$  in the reaction, and can be taken as a constant because  $\text{NH}_2\text{OH}$  is kept at a constant large excess in our experiment and does not affect the kinetics.  $n$  is the number of resazurin molecules adsorbed at the catalytic sites on a single nanoparticle surface. From Langmuir adsorption equilibrium,

$$n = n_T \theta_s = n_T \frac{K_1 [\text{S}]}{1 + K_1 [\text{S}]}$$

where  $n_T$  is the total number of catalytic sites on one nanoparticle surface,  $\theta_s$  is the fraction of occupied surface catalytic sites by the substrate, and  $K_1$  is the substrate adsorption equilibrium constant. Note here we are considering  $\tau_{\text{off}}$ , the waiting time for the formation of a product molecule, and before the event of product formation occurs, there is no product molecule yet on the nanoparticle surface; so the Langmuir adsorption equilibrium only contains the substrate term.

Let  $k = k_i k'$ , and then we have,

$$k_{\text{app}} = k n_T \theta_s = \frac{\gamma_{\text{eff}} K_1 [\text{S}]}{1 + K_1 [\text{S}]}$$

where  $\gamma_{\text{eff}} = k n_T$  and  $\gamma_{\text{eff}}$  here represents the combined reactivity of all surface catalytic sites on one Au-nanoparticle.

In conventional ensemble measurements where reactions of a large ensemble of colloidal Au-nanoparticles are measured in solution simultaneously, the kinetic rate equations for the  $\tau_{\text{off}}$  reaction are:

$$\frac{d[\text{Au}_m\text{S}_n]}{dt} = -k_{\text{app}} [\text{Au}_m\text{S}_n] \quad (\text{S1})$$

$$\frac{d[\text{Au}_m\text{S}_{n-1}-\text{P}]}{dt} = k_{\text{app}} [\text{Au}_m\text{S}_n] \quad (\text{S2})$$

where  $[\text{Au}_m\text{S}_n]$  is the concentration of Au-nanoparticles that do not carry any product, and  $[\text{Au}_m\text{S}_{n-1}-\text{P}]$  is the concentration of Au-nanoparticles on which one product molecule is generated.

Under conditions of single-nanoparticle measurements, although the concentration of the substrate [S] is still a valid description, the concentration of one nanoparticle is meaningless and needs to be replaced by the probability of the single nanoparticle<sup>S11</sup>. Then, equations S1 and S2 turn to:

$$\frac{dP_{\text{Au}_m\text{S}_n}(t)}{dt} = -k_{\text{app}} P_{\text{Au}_m\text{S}_n}(t) = -\frac{\gamma_{\text{eff}} K_1 [\text{S}]}{1 + K_1 [\text{S}]} P_{\text{Au}_m\text{S}_n}(t) \quad (\text{S3})$$



Under the assumptions of the Langmuir-Hinshelwood model where a fast substrate adsorption equilibrium is established at all time,  $\text{Au}_m\text{S}_{n-1}$  state will be quickly turned to the  $\text{Au}_m\text{S}_n$  state, as substrate molecules in the solution will quickly bind to an available site to maintain the equilibrium. Similarly as described above, we first write the conventional kinetic rate equations in concentration terms:

$$\frac{d[\text{Au}_m\text{S}_{n-1} - \text{P}]}{dt} = -(k_1^0 + k_3)[\text{Au}_m\text{S}_{n-1} - \text{P}] + k_{-1}[\text{Au}_m\text{S}_n - \text{P}] \quad (\text{S7})$$

$$\frac{d[\text{Au}_m\text{S}_n - \text{P}]}{dt} = k_1^0[\text{Au}_m\text{S}_{n-1} - \text{P}] - (k_2 + k_{-1})[\text{Au}_m\text{S}_n - \text{P}] \quad (\text{S8})$$

$$\frac{d[\text{Au}_m\text{S}_n]}{dt} = k_2[\text{Au}_m\text{S}_n - \text{P}] \quad (\text{S9})$$

$$\frac{d[\text{Au}_m\text{S}_{n-1}]}{dt} = k_3[\text{Au}_m\text{S}_{n-1} - \text{P}] \quad (\text{S10})$$

Where  $k_1^0 = k_1[\text{S}]$ . We then replace the concentration terms of nanoparticles with their probabilities. We get:

$$\frac{dP_{\text{Au}_m\text{S}_{n-1}-\text{P}}(t)}{dt} = -(k_1^0 + k_3)P_{\text{Au}_m\text{S}_{n-1}-\text{P}}(t) + k_{-1}P_{\text{Au}_m\text{S}_n-\text{P}}(t) \quad (\text{S11})$$

$$\frac{dP_{\text{Au}_m\text{S}_n-\text{P}}(t)}{dt} = k_1^0P_{\text{Au}_m\text{S}_{n-1}-\text{P}}(t) - (k_2 + k_{-1})P_{\text{Au}_m\text{S}_n-\text{P}}(t) \quad (\text{S12})$$

$$\frac{dP_{\text{Au}_m\text{S}_n}(t)}{dt} = k_2P_{\text{Au}_m\text{S}_n-\text{P}}(t) \quad (\text{S13})$$

$$\frac{dP_{\text{Au}_m\text{S}_{n-1}}(t)}{dt} = k_3P_{\text{Au}_m\text{S}_{n-1}-\text{P}}(t) \quad (\text{S14})$$

The initial conditions for solving the Equations S11-14 are

$$P_{\text{Au}_m\text{S}_{n-1}-\text{P}}(0) = 1, \quad P_{\text{Au}_m\text{S}_n-\text{P}}(0) = P_{\text{Au}_m\text{S}_n}(0) = P_{\text{Au}_m\text{S}_{n-1}}(0) = 0$$

with  $t = 0$  being the onset of each on-time  $\tau_{\text{on}}$ , and at any time within  $\tau_{\text{on}}$ ,  $P_{\text{Au}_m\text{S}_{n-1}-\text{P}}(t) + P_{\text{Au}_m\text{S}_n-\text{P}}(t) + P_{\text{Au}_m\text{S}_n}(t) + P_{\text{Au}_m\text{S}_{n-1}}(t) = 1$ .

We can then consider the probability density  $f_{\text{on}}(\tau)$  of the on-time  $\tau_{\text{on}}$ .  $\tau_{\text{on}}$  is the time required to finish reactions *ii* and *iii*, or the time required to finish reaction *iv*. The probability for finding a particular  $\tau$  is  $f_{\text{on}}(\tau)\Delta\tau$ , which is equal to the sum of (1) the probability of switching from the  $\text{Au}_m\text{S}_n-\text{P}$  state to the  $\text{Au}_m\text{S}_n$  state between the time  $\tau$  and  $\tau+\Delta\tau$  and (2) the probability of switching from the  $\text{Au}_m\text{S}_{n-1}-\text{P}$  state to the  $\text{Au}_m\text{S}_{n-1}$  state between the time  $\tau$  and  $\tau+\Delta\tau$ . The probability of switching from the  $\text{Au}_m\text{S}_n-\text{P}$  state to the  $\text{Au}_m\text{S}_n$  state between the time  $\tau$  and  $\tau+\Delta\tau$  is  $\Delta P_{\text{Au}_m\text{S}_n}(\tau)$ , which equals  $k_2P_{\text{Au}_m\text{S}_n-\text{P}}(\tau)\Delta\tau$ . The probability of switching from the  $\text{Au}_m\text{S}_{n-1}-\text{P}$  state to the  $\text{Au}_m\text{S}_{n-1}$  state between the time  $\tau$  and  $\tau+\Delta\tau$  is  $\Delta P_{\text{Au}_m\text{S}_{n-1}}(\tau)$ , which equals  $k_3P_{\text{Au}_m\text{S}_{n-1}-\text{P}}(\tau)\Delta\tau$ . Then  $f_{\text{on}}(\tau)$  is:

$$f_{\text{on}}(\tau) = \left. \frac{dP_{\text{Au}_m\text{S}_n}(t)}{dt} \right|_{t=\tau} + \left. \frac{dP_{\text{Au}_m\text{S}_{n-1}}(t)}{dt} \right|_{t=\tau} = k_2P_{\text{Au}_m\text{S}_n-\text{P}}(\tau) + k_3P_{\text{Au}_m\text{S}_{n-1}-\text{P}}(\tau).$$

Solving Equations S11-14 for  $P_{\text{Au}_m\text{S}_n-\text{P}}(\tau)$  and  $P_{\text{Au}_m\text{S}_{n-1}-\text{P}}(\tau)$  by Laplace transform with the initial conditions, we obtain:

$$f_{\text{on}}(\tau) = \frac{(k_2 k_1^0 + k_3 a + k_3 b + k_3 k_{-1} + k_3 k_2) e^{(b+a)\tau}}{2a} + \frac{(-k_2 k_1^0 + k_3 a - k_3 b - k_3 k_{-1} - k_3 k_2) e^{(b-a)\tau}}{2a} \quad (\text{S15})$$

with  $a = \sqrt{\frac{1}{4}(k_{-1} + k_1^0 + k_2 + k_3)^2 - (k_{-1} k_3 + k_2 k_1^0 + k_2 k_3)}$ , and  $b = -\frac{1}{2}(k_{-1} + k_1^0 + k_2 + k_3)$ .

Then  $\langle \tau_{\text{on}} \rangle^{-1}$ , which represents the time-averaged product dissociation rate for a *single nanoparticle*, is,

$$\begin{aligned} \langle \tau_{\text{on}} \rangle^{-1} &= 1 / \int_0^{\infty} f_{\text{on}}(\tau) d\tau \\ &= \frac{(k_{-1} k_3 + k_2 k_1^0 + k_2 k_3)^2}{k_3 (k_{-1}^2 + k_2^2 + 2k_{-1} k_2 + k_1^0 k_{-1}) + k_1^0 k_2 (k_{-1} + k_2 + k_1^0 + k_3)} \\ &= \frac{k_2 K_2 [\text{S}] + k_3}{1 + K_2 [\text{S}]} \end{aligned} \quad (\text{S16})$$

where  $K_2 = \frac{k_1}{k_{-1} + k_2}$ . Equation S16 is given as Equation (2) in the main text. Consider the limiting conditions for  $\langle \tau_{\text{on}} \rangle^{-1}$ . When  $[\text{S}] \rightarrow 0$ ,

$$\langle \tau_{\text{on}} \rangle_{[\text{S}] \rightarrow 0}^{-1} = \frac{k_2 K_2 [\text{S}] + k_3}{1 + K_2 [\text{S}]} = k_3$$

When  $[\text{S}] \rightarrow \infty$ ,

$$\langle \tau_{\text{on}} \rangle_{[\text{S}] \rightarrow \infty}^{-1} = \frac{k_2 K_2 [\text{S}] + k_3}{1 + K_2 [\text{S}]} = k_2$$

To give a physical interpretation of [S] dependence of  $\langle \tau_{\text{on}} \rangle^{-1}$ , when  $[\text{S}] \rightarrow 0$ , the forward reaction of reaction *ii* is extremely slow ( $k_1[\text{S}] = 0$ , Figure S14), then the product dissociation dominantly takes the direct dissociation pathway (reaction *iv*) and the reaction rate is determined by  $k_3$ , the rate constant for direct product dissociation. When  $[\text{S}] \rightarrow \infty$ , the  $\text{Au}_m\text{S}_{n-1}\text{-P}$  state will be immediately converted to the  $\text{Au}_m\text{S}_n\text{-P}$  state via reaction *ii* due to the large value of  $k_1[\text{S}]$ ; then the product dissociation will dominantly take the substrate-assisted pathway and the reaction rate is determined by  $k_2$ , the reaction *iii*.

With different relative magnitudes between  $k_2$  and  $k_3$ , Equation S16 immediately predicts three types of [S] dependence of  $\langle \tau_{\text{on}} \rangle^{-1}$ . 1) Type-I: when  $k_2 > k_3$ ,  $\langle \tau_{\text{on}} \rangle^{-1}$  will increase with increasing [S] and eventually saturates. 2) Type-II: when  $k_2 < k_3$ , the  $\langle \tau_{\text{on}} \rangle^{-1}$  will decrease with increasing [S] and flattens. 3) Type-III: when  $k_2 = k_3$ , or  $k_1 = 0$ , or  $K_2 = 0$  (the latter two cases represent the complete shut down of the substrate-assisted pathway for product dissociation),  $\langle \tau_{\text{on}} \rangle^{-1}$  will be independent of [S]. Figure S15 show the simulations of these three behaviors of  $\langle \tau_{\text{on}} \rangle^{-1}$ . All these three types of behaviors have been observed in our single-nanoparticle catalysis measurements (Fig. 3).

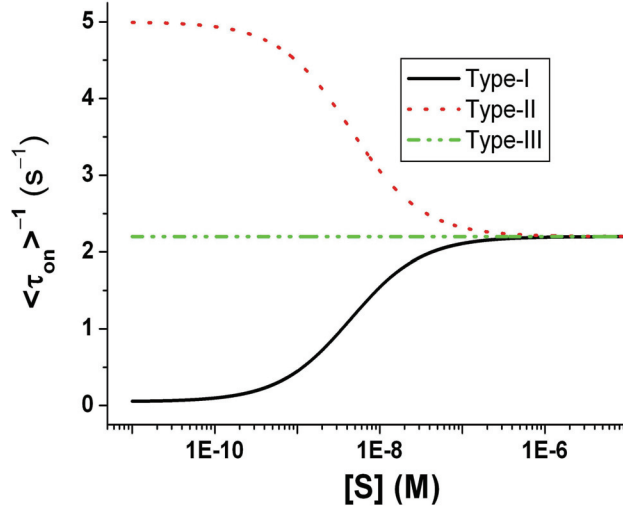


**Figure S15.** Three types of possible substrate concentration dependence of  $\langle \tau_{\text{on}} \rangle^{-1}$ . The parameters for type-I:  $k_{-1}=0.001 \text{ s}^{-1}$ ,  $k_1=5 \times 10^8 \text{ s}^{-1}\text{M}^{-1}$ ,  $k_2=2.2 \text{ s}^{-1}$ ,  $k_3=0.05 \text{ s}^{-1}$ ; type-II:  $k_{-1}=0.001 \text{ s}^{-1}$ ,  $k_1=5 \times 10^8 \text{ s}^{-1}\text{M}^{-1}$ ,  $k_2=2.2 \text{ s}^{-1}$ ,  $k_3=5 \text{ s}^{-1}$ ; type-III:  $k_{-1}=\text{a.n.}$ ,  $k_1=\text{a.n.}$ ,  $k_2=2.2 \text{ s}^{-1}$ ,  $k_3=2.2 \text{ s}^{-1}$  or  $k_{-1}=\text{a.n.}$ ,  $k_1=0.$ ,  $k_2=\text{a.n.}$ ,  $k_3=2.2 \text{ s}^{-1}$ . a.n. = arbitrary number.

**Part C: The overall rate of turnovers.**

With Equations S6 and S16, we can get the overall rate of turnovers of the catalysis for a single nanoparticle,  $\langle \tau_{\text{off+on}} \rangle^{-1}$ , i.e., the number of turnovers per unit time per particle,

$$\begin{aligned} \langle \tau_{\text{off+on}} \rangle^{-1} &= \langle \tau_{\text{off}} + \tau_{\text{on}} \rangle^{-1} = \left( \langle \tau_{\text{off}} \rangle + \langle \tau_{\text{on}} \rangle \right)^{-1} \\ &= \frac{\gamma_{\text{eff}} k_2 K_1 K_2 [S]^2 + \gamma_{\text{eff}} k_3 K_1 [S]}{(\gamma_{\text{eff}} + k_2) K_1 K_2 [S]^2 + (\gamma_{\text{eff}} K_1 + k_3 K_1 + k_2 K_2) [S] + k_3} \end{aligned} \quad (\text{S17})$$

At  $[S] = 0$ ,  $\langle \tau_{\text{off+on}} \rangle_{[S]=0}^{-1} = 0$  and no catalysis occurs; at  $[S] \rightarrow \infty$ ,  $\langle \tau_{\text{off+on}} \rangle_{[S] \rightarrow \infty}^{-1} = \gamma_{\text{eff}} k_2 / (\gamma_{\text{eff}} + k_2)$ , which reduces to  $\gamma_{\text{eff}}$  when the catalytic conversion reaction is rate-limiting in the catalytic cycle (i.e.,  $\gamma_{\text{eff}} \ll k_2$ ). Figure S16 shows the  $[S]$  dependence of  $\langle \tau_{\text{off+on}} \rangle^{-1}$ , which shows a saturation kinetics.

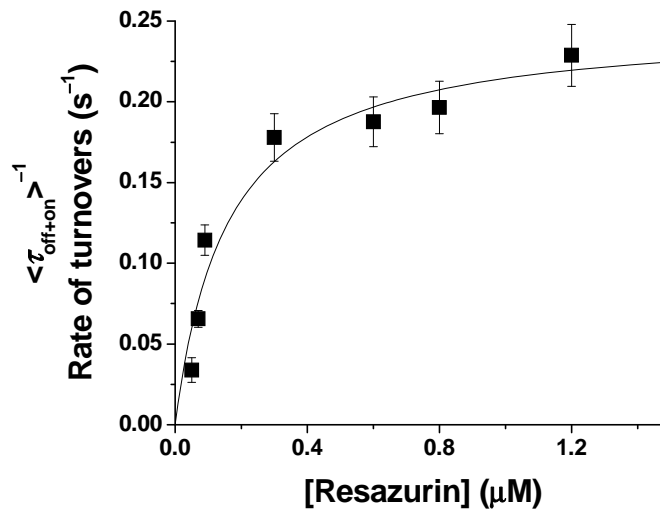


**Figure S16.** Simulation (solid line) of the [S] dependence of  $\langle \tau_{\text{off+on}} \rangle^{-1}$ , the rate of turnovers. Kinetic parameters are taken from the fits in Figure 2a and b:  $\gamma_{\text{eff}} = 0.28 \text{ s}^{-1}$ ,  $K_1 = 6 \text{ }\mu\text{M}^{-1}$ ,  $k_2 = 2.2 \text{ s}^{-1}$ ,  $K_2 = 16 \text{ }\mu\text{M}^{-1}$ , and  $k_3 = 0 \text{ s}^{-1}$ . Data points are experimental results.

## 19. Further discussions of the kinetic mechanism.

Reaction *i*. This reaction is the catalytic conversion of resazurin to resorufin. The conversion of resazurin to resorufin involves an N–O bond cleavage, and is thus taken as irreversible.

Reaction *ii*. This reaction is necessitated by the concentration dependence of  $\langle \tau_{\text{on}} \rangle^{-1}$ , which indicates the substrate must participate in the product dissociation in one of the reaction pathways. This reaction does not have to be reversible to fit our data satisfactorily. The reversibility is nevertheless used here because it is related to substrate adsorption-desorption equilibrium.

Reaction *iii*. This reaction is the final dissociation of product in the substrate-assisted product dissociation pathway. It is taken as irreversible considering the miniature amount of product present in the reaction solution, and the constant carrying away of the product by the solution flow.

Furthermore, in our control experiment with Au-nanoparticles and pure resorufin, no resorufin binding/unbinding was observed, which would show on-off fluorescence intensity trajectories. The binding process of resorufin to Au-nanoparticles is thus negligible.

Reaction *iv*. This reaction is the direct dissociation of the product after the catalytic conversion step, which is needed along with reactions *ii* and *iii* to account for the heterogeneous [S] dependence of  $\langle \tau_{\text{on}} \rangle^{-1}$ . It is taken as irreversible for the same reason as reaction *iii*, as described above.

## 20. Studies on different-sized Au-nanoparticles.

Using our single-nanoparticle single-turnover approach, we further studied the 2-nm and 10-nm Au-nanoparticles. For 2-nm Au-nanoparticles, we did not observe digital, stochastic fluorescence burst trajectories, consistent with ensemble measurements that they are not active in catalyzing the reduction of resazurin to resorufin by  $\text{NH}_2\text{OH}$  (see Section 3 above).

For 10-nm Au-nanoparticles, we observed catalysis in the single-nanoparticle experiment. An exemplary single-turnover fluorescence trajectory of a single 10-nm Au-nanoparticle is shown in Figure S17A. The resazurin concentration dependence of  $\langle \tau_{\text{off}} \rangle^{-1}$  and  $\langle \tau_{\text{on}} \rangle^{-1}$  are shown in Figure S17B, C, in comparison with those of the 6-nm Au-nanoparticles. The activity differences between the 10-nm and 6-nm Au-nanoparticles are obvious in both the off-time reaction, i.e., catalysis, and the on-time reaction, i.e., product dissociation.

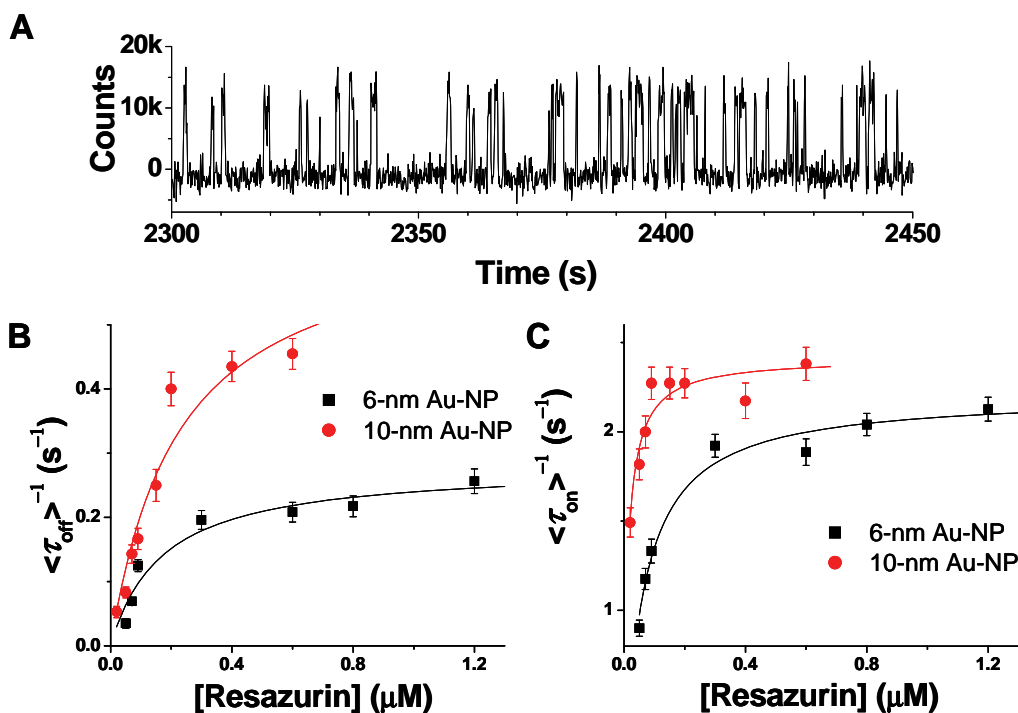


**Figure S17.** (A) A segment of an exemplary single-turnover fluorescence catalysis trajectory of a single 10-nm Au-nanoparticle at [resazurin] = 0.05  $\mu\text{M}$  and  $[\text{NH}_2\text{OH}] = 1 \text{ mM}$ . (B, C) Resazurin concentration titrations of nanoparticle-averaged  $\langle \tau_{\text{off}} \rangle^{-1}$  and  $\langle \tau_{\text{on}} \rangle^{-1}$  of single 10-nm Au-nanoparticles. Data of 6-nm Au-nanoparticles are taken from Figure 2a, b. Fitting the 10-nm Au-nanoparticle data with Equations (1) and (2) gives  $\gamma_{\text{eff}} = 0.7 \pm 0.1 \text{ s}^{-1}$ ,  $K_1 = 4 \pm 2 \mu\text{M}^{-1}$ ,  $k_2 = 2.4 \pm 0.1 \text{ s}^{-1}$ ,  $K_2 = 55 \pm 60 \mu\text{M}^{-1}$ , and  $k_3 = 0.5 \pm 1.2 \text{ s}^{-1}$ .

## 21. Possible contribution of impurity adsorption/desorption to activity fluctuations.

It is possible that the adsorption/desorption of impurity molecules to the active sites could inhibit and thus affect the activity of Au nanoparticles. Then the adsorption/desorption dynamics of the impurity could lead to activity fluctuations of Au nanoparticles. If this is the main cause of activity fluctuations, the activity fluctuation timescale would be determined by the timescale of the adsorption/desorption dynamics of impurity molecules — (1) If the rate-limiting step in the impurity adsorption/desorption is the desorption process, then the rate of desorption would determine the rate of activity fluctuation, and should be independent of impurity concentration assuming direct desorption. (2) If the rate-limiting step is the adsorption process, then the rate of adsorption would determine the rate of activity fluctuation, and should be linearly proportional to the impurity concentration assuming that the adsorption follows first order kinetics. (3) If the rates of adsorption and desorption are comparable, then the contribution of the adsorption component should still give a linear dependence of the activity fluctuation rate on the impurity concentration.

However, we think that the impurity adsorption/desorption dynamics is likely not the *main cause* for the activity fluctuations because of the following:

- (1) If there is impurity, it could be from the solvent (water),  $\text{NH}_2\text{OH}$ , or resazurin. If the impurity is from water (note we use nanopure water) or  $\text{NH}_2\text{OH}$ , its concentration is then

constant in our experiments because the concentrations of water and  $\text{NH}_2\text{OH}$  are kept constant. Then the timescales of the impurity adsorption/desorption dynamics would be constant regardless of the rate of turnovers where we merely vary the resazurin concentration, and so would be the timescales of activity fluctuations. In contrast, our data show that the rate (i.e., inverse of timescale) of activity fluctuations are not constant across different substrate concentrations (Figure 4d and Figure below).

(2) If the impurity is from resazurin, then its concentration would be linearly proportional to the resazurin concentration. If impurity desorption is rate-limiting, then the rate of the resulted activity fluctuation would be independent of its concentration and thus independent of resazurin concentration, which is against our observation (Figure below). If impurity adsorption is rate-limiting or adsorption/desorption rates are comparable, then the rate of the resulted activity fluctuation would be linearly proportional to its concentration and thus to resazurin concentration. In contrast, the observed dependence is clearly nonlinear.

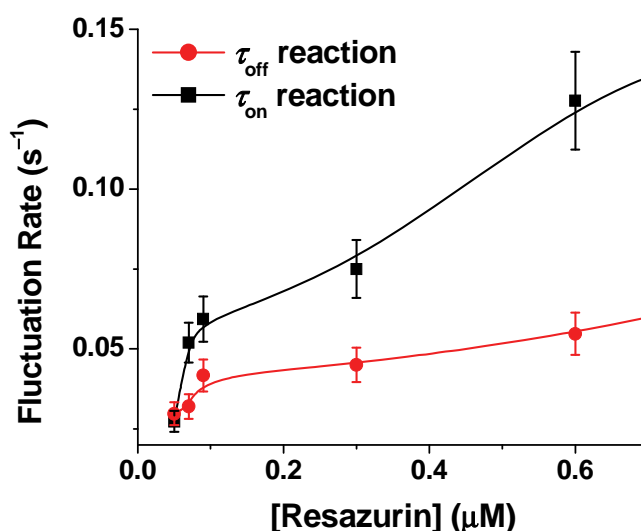


**Figure S18.** Resazurin concentration dependence of the activity fluctuation rate of 6-nm Au nanoparticles.

Nevertheless, the impurity adsorption/desorption could also contribute to the surface restructuring dynamics, which we attribute as the underlying causes of the activity fluctuations, but is likely not the main contributor as we discussed above.

## Acknowledgements

This work is supported by Cornell University, American Chemical Society Petroleum Research Foundation, and Cornell Center for Materials Research. We thank John Grazul for assistance in TEM measurements. The TEM facility at the Cornell Center of Materials Research is supported by the National Science Foundation.

## References

- S1. Handley, D. A. in *Colloidal gold: Principles, methods, and applications* (ed. Hayat, M. A.) 13-32 (Academic Press, Inc., San Diego, 1989).

- S2. Natan, M. J. & Lyon, L. A. in *Metal nanoparticles: Synthesis, characterization, and application* (eds. Feldheim, D. L. & Foss, C. A., Jr.) 183-205 (Marcel Dekker, Inc., New York, 2002).
- S3. Grabar, K. C., Freeman, R. G., Hommer, M. B. & Natan, M. J. Preparation and characterization of au colloid monolayers. *Anal. Chem.* **67**, 735-743 (1995).
- S4. Beckwith, R., Cooper, J. & Margerum, D. Kinetics and mechanism of the oxidation of hydroxylamine by aqueous bromine. *Inorg. Chem.* **33**, 5144-5150 (1994).
- S5. Haugland, R. P. *The handbook: A guide to fluorescent probes and labeling technologies* (Invitrogen Corp, 2005).
- S6. Villegas, L. et al. Aqueous photopolymerization with visible-light photoinitiators: Acrylamide polymerization photoinitiated with a phenoxazine dye/amine system. *Journal of Polymer Science: Part A: Polymer Chemistry* **39**, 4074-4082 (2001).
- S7. Macklin, J. J., Trautman, J. K., Harris, T. D. & Brus, L. E. Imaging and time-resolved spectroscopy of single molecules at an interface. *Science* **272**, 255-258 (1996).
- S8. Cheng, P. P. H. et al. Dynamic and static quenching of fluorescence by 1-4 nm diameter gold monolayer-protected clusters. *J. Phys. Chem. B* **110**, 4637-4644 (2006).
- S9. Lakowicz, J. R. *Principles of fluorescence spectroscopy* (Kluwer Academic/Plenum Publisher, New York, 1999).
- S10. Satterfield, C. N. *Heterogeneous catalysis in practice* (McGraw-Hill Book Company, New York, 1980).
- S11. Xie, X. S. Single-molecule approach to enzymology. *Single Mol.* **2**, 229-236 (2001).